

Robot Trajectory Planning With QoS Constrained IRS-assisted Millimeter-Wave Communications

Cristian Tatino, *Student Member, IEEE*, Nikolaos Pappas, *Member, IEEE*, and Di Yuan, *Senior Member, IEEE*

Abstract—This paper considers the joint optimization of trajectory and beamforming of a wirelessly connected robot using intelligent reflective surface (IRS)-assisted millimeter-wave (mm-wave) communications. The goal is to minimize the motion energy consumption subject to time and communication quality of service (QoS) constraints. This is a fundamental problem for industry 4.0, where robots may have to maximize their battery autonomy and communication efficiency. In such scenarios, IRSs and mm-waves can dramatically increase the spectrum efficiency of wireless communications providing high data rates and reliability for new industrial applications.

We present a solution to the optimization problem that first exploits mm-wave channel characteristics to decouple beamforming and trajectory optimizations. Then, the latter is solved by a successive-convex optimization (SCO) algorithm. The algorithm takes into account the obstacles' positions and a radio map and provides solutions that avoid collisions and satisfy the QoS constraint. Moreover, we prove that the algorithm converges to a solution satisfying the Karush-Kuhn-Tucker (KKT) conditions.

I. INTRODUCTION

Robotic and wireless technologies are playing a crucial role in Industry 4.0. leading to full automation of manufacturing processes, warehousing, and logistics [1]. In such scenarios, an increasing number of robots and the rising of new industrial applications, such as augmented and virtual reality for assisted manufacturing, may require Gbps peak data rates [2]. Millimeter-wave (mm-wave) communications can provide a huge amount of bandwidth for satisfying data rate requirements for industrial applications [3]. However, high blockage sensitivity reduces communication reliability while robots move in environments with obstacles. These must be avoided by the robot trajectory, which highly affects mm-wave performance as it determines whether the robot is in line-of-sight (LOS) or non-line-of-sight (NLOS).

To enhance coverage in mm-waves scenarios, intelligent reflective surfaces (IRSs) have been proposed [4]. IRSs consist of arrays of passive reflective elements that, by adjusting phase shifters, can reflect the incident signal from the transmitter to the receiver without incurring in additional received noise. This represents a low-cost solution to provide alternative paths to the direct link in case of blockages. However, phase shifters must be set according to the channel that depends on the robot trajectory. Moreover, robots have tasks that are usually characterized by stringent deadlines and are equipped with batteries that limit the operational time and

productivity. When a robot is out of energy, its battery must be charged with a cost of time and power. Hence, in this work, we consider wirelessly connected robots in IRS-assisted mm-wave scenarios, where trajectory and beamforming are optimized to minimize the motion energy consumption and satisfy collision avoidance, time, and QoS constraints.

Energy minimization has been one of the most important problems in robot trajectory optimization [5], [6]. In [5], the authors show up to 50% of energy-saving when an optimal control of the robot's speed is performed. Wirelessly connected robots are considered in [6] that proposes a joint robot communication and motion energy minimization by controlling transmit power and robot's speed along a fixed trajectory. However, the potentials of mm-waves transmissions for wirelessly connected robots need to be further explored, even though some studies have been performed for unmanned aerial vehicle (UAV) scenarios [7]. UAV and IRSs are considered in [8] that propose a joint trajectory and IRS beamforming optimization to maximize the average achievable rate at the users. However, especially in mm-wave scenarios, UAV communications do not present the same characteristics of robots. More precisely, thanks to the possibility to control the altitude, UAVs can avoid most of the obstacles and NLOS conditions.

A. Contributions

In this paper, we consider a novel robot trajectory optimization problem with quality of service (QoS) constrained IRS-assisted mm-wave communications. Specifically, the problem aims to minimize motion energy consumption while avoiding collisions with obstacles, and satisfying minimum average data rate and time constraints to reach the final position. To the best of our knowledge, energy-efficient trajectory planning problems for wirelessly connected robots have not been considered in mm-wave industrial scenarios. We consider the mutual effects of joint trajectory and beamforming optimization on the energy consumption and achieved data rate. We propose a successive convex optimization (SCO) algorithm that can find feasible trajectories by using a radio map and environment information. We prove that the algorithm converges to a point satisfying KKT conditions, and we show the results for several system parameters. Moreover, we show how IRSs, by enhancing the coverage, can increase the robot motion energy efficiency.

II. SYSTEM MODEL

We consider an industrial scenario, e.g., an industrial plant, where a robot moves from a starting position q_s to its goal q_d within a time horizon of fixed duration. The robot moves

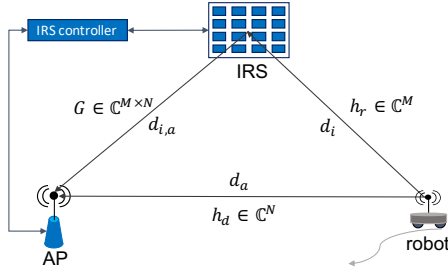


Fig. 1: A scenario consisting of an IRS-aided robot uplink communication.

on the horizontal plane of a restricted area characterized by the presence of 3D obstacles. These are represented by a set \mathcal{O} of cylinders with elliptic bases and given heights. Note that an arbitrarily shaped obstacle can be approximated by the intersection and the union of several convex shapes [9]. The area is covered by an AP using mm-waves to which the robot needs to transmit uplink data by maintaining a minimum average rate requirement (r_{min}). The robot is equipped with a single antenna, whereas, the AP is equipped with a uniform linear array with N antennas. The robot-AP communication is assisted by an IRS consisting of M reflective elements. These are managed by a controller, which shares the channel state information with the AP. A scheduler, which we assume to be co-located with the controller, optimizes the robot trajectory and the beamforming to minimize the motion energy consumption. We consider both active and passive beamforming at the AP and IRS, respectively. Hereafter, we consider the following notations: $(\cdot)^T$ and $(\cdot)^H$, represents the transpose and the conjugate transpose, respectively; $diag(\cdot)$ returns the diagonalization of a vector and $arg(\cdot)$ denotes the phase of a complex number. Finally, $\|\cdot\|_n$ represents the n -norm.

The robot must avoid collisions with obstacles and reach the destination within a deadline. We divide the time horizon in K timeslots, $k = 0, \dots, K$, of duration Δ_t . In each timeslot, we assume that the location of the robot and channel conditions do not change. Moreover, within a timeslot, the robot can travel for a maximum distance of $D_{max} = v_{max}\Delta_t$, where, v_{max} is the maximum speed. A trajectory of the robot can be represented as a sequence $\mathbf{q} = [q_0, q_1, \dots, q_K]$, where $q_0 = q_s$ and $q_K = q_d$. The term $q_k = [x_k, y_k]$, $k = 0, \dots, K$, represents the Cartesian coordinates of the robot on the horizontal plane in the k -th timeslot. Let $q_a = [x_a, y_a]$ and $q_i = [x_i, y_i]$ represents the fixed positions of the AP and the IRS, respectively. The altitude of the robot is fixed at its antenna height z_r , whereas z_a represents the height at which the AP is installed and z_i the height of the IRS. Let v_k be the speed of the robot at the k -th timeslot, then, the motion energy consumption for DC motor-equipped robot along the path can be written as in [6]:

$$E = \sum_{k=1}^{k=K} E_k = \sum_{k=1}^{k=K} c_1 v_k^2 \Delta_t + c_2 v_k \Delta_t + c_3 \Delta_t = \sum_{k=1}^{k=K} c_1 \frac{\|q_k - q_{k-1}\|_2^2}{\Delta_t} + c_2 \|q_k - q_{k-1}\|_2 + c_3 \Delta_t, \quad (1)$$

where, E_k is the energy consumption in the k -th timeslot, and c_1 , c_2 , and c_3 are positive constants depending on the characteristics of the robot and external load.

A. Channel Model

As shown in Fig. 1, let $h_r \in \mathbb{C}^M$ be the channel vector between the robot and the IRS and $G \in \mathbb{C}^{M \times N}$ denote the channel matrix between the IRS and the AP. The direct channel between the AP and the robot is represented by vector $h_d \in \mathbb{C}^M$. Then, the received baseband signal at the AP in timeslot k can be written as follows:

$$y_k = (h_{r,k}^H \Phi_k G_k + h_{d,k}^H) w_k \sqrt{p_t} s_k + \eta_k, \quad (2)$$

where, s_k and p_t are the transmit signal and the transmit power in the uplink, respectively, $\eta_k \sim \mathcal{CN}(0, \sigma^2)$ denotes the additive white Gaussian noise (AWGN). The term $w_k \in \mathbb{C}^M$ is the normalized beamforming vector at the AP, and $\Phi_k = \text{diag}(e^{j\theta_{1,k}}, \dots, e^{j\theta_{M,k}})$ is a diagonal matrix that accounts for the phase shifts $\theta_{m,k} \in [0, 2\pi]$ associated with reflective elements of the IRS. Due to the high path loss of mm-wave transmissions, signals that are reflected more than once are subject to severe attenuations and are not considered in (2). Thus, the received signal-to-noise ratio (SNR) at timeslot k can be written as follows:

$$\text{SNR}_k = \frac{|(h_{r,k}^H \Phi_k G_k + h_{d,k}^H) w_k|^2}{\sigma^2} p_t, \quad (3)$$

where, the superscript H represents the hermitian. Moreover, let $d_{i,k} = \sqrt{(z_r - z_i)^2 + \|q_k - q_i\|_2^2}$, and $d_{a,k} = \sqrt{(z_r - z_a)^2 + \|q_k - q_a\|_2^2}$ be the robot-IRS and robot-AP distances, respectively. Then, channel vectors $h_{r,k}$ and $h_{d,k}$ can be modeled as follows:

$$h_{r,k} = \sqrt{\rho d_{i,k}^{-\nu}} \tilde{h}_{r,k}, \quad (4) \quad h_{d,k} = \sqrt{\rho d_{a,k}^{-\mu}} \tilde{h}_{d,k}, \quad (5)$$

where, $\tilde{h}_{r,k} \sim \mathcal{CN}(0, I)$ and $\tilde{h}_{d,k} \sim \mathcal{CN}(0, I)$ are complex gaussian vectors whose elements are independent and identical distributed (i.i.d) with zero means and unit variances. The term ρ is the path loss at the reference distance of 1 m, and ν and μ are the path loss exponents of the reflected and direct channels, respectively.

Finally, let $\mathbf{r} = [r_0, r_1, \dots, r_K]$ be a vector, the elements of which represent the rates at timeslots $k = 0, 1, \dots, K$. Thus, by using the Shannon's formula, the average rate (\bar{r}) for a trajectory \mathbf{q} is given by:

$$\bar{r} = \frac{1}{K} \sum_{k=0}^K r_k = \frac{B_w}{K} \sum_{k=0}^K \log_2(1 + \text{SNR}_k) = \frac{B_w}{K} \times \sum_{k=0}^K \log_2 \left(1 + \frac{|(\sqrt{\rho d_{i,k}^{-\nu}} \tilde{h}_{r,k}^H \Phi_k G_k + \sqrt{\rho d_{a,k}^{-\mu}} \tilde{h}_{d,k}^H) w_k|^2}{\sigma^2} p_t \right), \quad (6)$$

where, (4) and (5) are used in (3) and B_w represents the system bandwidth. We can observe that \bar{r} is a function of Φ_k , w_k , and q_k . The latter is included in $d_{i,k}$, and $d_{a,k}$. Thus, the robot's position and beamforming affect the rate, which

in turn affects the trajectory. In the next section, we formulate the problem of minimizing motion energy consumption, maintaining a certain minimum average rate considering both the beamforming and trajectory optimization.

III. PROBLEM FORMULATION

In this section, we formulate the problem introduced in Section II. Let $\Phi = [\Phi_0, \Phi_1, \dots, \Phi_K]$ and $w = [w_0, w_1, \dots, w_K]$, then the joint robot trajectory and beamforming problem can be formulated as follows:

$$P1 : \min_{\mathbf{q}, \Phi, \mathbf{w}} E \quad (7a)$$

$$\text{s.t. } \bar{r} \geq r_{min}, \quad (7b)$$

$$\|q_k - q_{k-1}\|_2 \leq D_{max}, \quad k = 1, \dots, K, \quad (7c)$$

$$q_0 = q_s, \quad q_K = q_d, \quad (7d)$$

$$(q_k - q_{c,o})^T P_o^{-1} (q_k - q_{c,o}) \geq d_s, \quad \forall k, \forall o \in \mathcal{O}, \quad (7e)$$

$$\|w_k\|_2^2 \leq 1, \quad \forall k, \quad (7f)$$

$$\Phi_k = \text{diag}(e^{j\theta_{1k}}, \dots, e^{j\theta_{Mk}}), \quad \forall k, \quad (7g)$$

$$0 \leq \theta_{m,k} \leq 2\pi, \quad \forall m, \forall k, \quad (7h)$$

where, the objective function (7a) represents the total robot motion energy consumption along the trajectory given by (1). The first constraint (7b) represents the QoS requirement to complete the task, where \bar{r} is defined in (6) and r_{min} is the minimum required average rate. Constraints (7c) allow the robot to move in a timeslot for a maximum distance of D_{max} , whereas (7d) fix the starting and the goal positions. To avoid collisions with obstacles, we include (7e). As described in Section II, each obstacle $o \in \mathcal{O}$ is characterized by an ellipsoid shape on the horizontal plane, with a center $q_{c,o}$, and a symmetric and positive definite matrix P_o . The latter defines the length of the axis and the rotation of the ellipse, and $d_s \geq 1$ represents a safety distance between the robot and the obstacle. Constraints (7f) and (7h) impose the norm of w_k to be at most one and $\theta_{m,k}$ to be continuous, respectively.

Problem $P1$ is non-linear and non-convex. However, we show that, for each robot trajectory \mathbf{q} , it is possible to find closed-forms of Φ and \mathbf{w} that maximize the average rate. More precisely, Φ_k and w_k are not contributing to the cost in (7a). Thus, when the right-hand side (RHS) of (7b) is maximized given a certain trajectory, we obtain a problem with a larger feasible region, of which the optimum is equivalent to that of $P1$. This equivalent problem of constrained trajectory optimization is solved in Section IV by using an SCO algorithm.

A. Average Rate Maximization

In this section, we first find closed-form solutions of Φ and \mathbf{w} that maximize the average rate \bar{r} for a fixed trajectory by solving the following problem:

$$P2 : \max_{\Phi, \mathbf{w}} \bar{r} \quad (8a)$$

$$\text{s.t. (7f), (7g), (7h),}$$

where, \bar{r} is given by (6). We can assume that the IRS and the AP are installed with LOS between them. Since in mm-wave communications the LOS path presents a much higher

gain than the sum of NLOS paths, the IRS-AP channel at timeslot k can be approximated by a rank-one matrix [4]: $G_k = \sqrt{NM}\gamma\tilde{a}_k\tilde{b}_k^T$, where, $\gamma = \sqrt{\rho d_{ia}^{-2}}$, and d_{ia} is the AP-IRS distance that is fixed and does not depend on q_k . The path loss exponent that is associated with the LOS path between the AP and the IRS is two. The terms $\tilde{a}_k \in \mathbb{C}^M$ and $\tilde{b}_k \in \mathbb{C}^N$ are the normalized array response vectors in timeslot k associated with the IRS and the AP, respectively.

Maximizing $P2$ is equivalent to maximizing the received SNR in each timeslot k (3). Assuming $\Phi_k = e^{\alpha_k}\hat{\Phi}_k$, this problem has a closed-form solution [4]:

$$\alpha_k^* = -\arg\left(\left(\tilde{b}_k^T\right)^H \tilde{h}_{d,k}\right), \quad (9)$$

$$\hat{\Phi}_k^* = \text{diag}\left(e^{-j\arg(g_{1,k})}, \dots, e^{-j\arg(g_{M,k})}\right), \quad (10)$$

$$w_k^* = \frac{\left(e^{\alpha_k^*}\sqrt{\rho d_{i,k}^{-\nu}}\tilde{h}_{r,k}^H\hat{\Phi}_k^*G_k + \sqrt{\rho d_{a,k}^{-\mu}}\tilde{h}_{d,k}^H\right)^H}{\|e^{\alpha_k^*}\sqrt{\rho d_{i,k}^{-\nu}}\tilde{h}_{r,k}^H\hat{\Phi}_k^*G_k + \sqrt{\rho d_{a,k}^{-\mu}}\tilde{h}_{d,k}^H\|_2}, \quad (11)$$

where, $g_k = \sqrt{\rho d_{ia}^{-2}}(\tilde{h}_{r,k}^* \circ \tilde{a}_k)$ and (\circ) denotes the elementwise product. By putting (9), (10), and (11) into (3), we obtain the following optimal SNR expression for timeslot k :

$$\begin{aligned} \text{SNR}_k^* &= \left(N|\rho|\gamma|^2\|\tilde{h}_{r,k}\|_1^2 d_{i,k}^{-\nu} + \right. \\ &2\sqrt{N}|\rho|\gamma\|\tilde{h}_{r,k}^H\|_1\|\tilde{b}_k^T\tilde{h}_{d,k}\| d_{i,k}^{-\nu/2}d_{a,k}^{-\mu/2} + \rho\|\tilde{h}_{d,k}\|_2^2 d_{a,k}^{-\mu}\left.)\frac{P_t}{\sigma^2} = \right. \\ &\left.(Ad_{i,k}^{-\nu} + Bd_{i,k}^{-\nu/2}d_{a,k}^{-\mu/2} + Cd_{a,k}^{-\mu}\right)\frac{P_t}{\sigma^2}, \end{aligned} \quad (12)$$

where, in the last equality, we have highlighted the dependence of SNR_k^* on the robot position q_k through the terms $d_{a,k}$ and $d_{i,k}$. However, ν and μ depend on the scattering environment. For this reason, starting from (12), we estimate ν , μ , and other parameters, i.e., A , B , and C , by fitting (12) with a radio map. The radio map provides the averaged optimal SNR^* for each position that is obtained by computing (9), (10), and (11) from a set of channel measurements. This procedure results in:

$$\widehat{\text{SNR}}_k^* = \left(\hat{A}d_{i,k}^{-\hat{\nu}} + \hat{B}d_{i,k}^{-\hat{\nu}/2}d_{a,k}^{-\hat{\mu}/2} + \hat{C}d_{a,k}^{-\hat{\mu}}\right)\frac{P_t}{\sigma^2}, \quad (13)$$

where, \hat{A} , \hat{B} , \hat{C} , $\hat{\nu}$, and $\hat{\mu}$ are the estimated parameters.

We can use (13) in (6) to obtain an estimation of the maximum rate resulting from the beamforming optimization:

$$\bar{r}^* = \frac{1}{K} \sum_{k=0}^K r_k^* = \frac{B_w}{K} \sum_{k=0}^K \log_2\left(1 + \widehat{\text{SNR}}_k^*\right) = \quad (14)$$

$$\frac{B_w}{K} \sum_{k=0}^K \log_2\left(1 + \left(\hat{A}d_{i,k}^{-\hat{\nu}} + \hat{B}d_{i,k}^{-\hat{\nu}/2}d_{a,k}^{-\hat{\mu}/2} + \hat{C}d_{a,k}^{-\hat{\mu}}\right)\frac{P_t}{\sigma^2}\right),$$

where, r_k^* is the optimized rate at timeslot k . Finally, by replacing the RHS of (7b) with (14), we can decouple the beamforming and the trajectory optimization obtaining the following problem:

$$P3 : \min_{\mathbf{q}, \Phi, \mathbf{w}} E \quad (15a)$$

$$\text{s.t. } \bar{\mathbf{r}}^* \geq \mathbf{r}_{min}, \quad (15b)$$

$$(7c), (7d), (7e),$$

where, E in (19a) is the robot energy consumption that is given by (1). This problem is equivalent to P1, but it considers the estimated maximum rate, $\bar{\mathbf{r}}^*$.

IV. TRAJECTORY OPTIMIZATION

In this section, we provide an algorithm to solve trajectory optimization problem $P3$. We first derive the following lemma:

Lemma 1: Given $c_1 \geq 0$, $c_2 \geq 0$, and $c_3 \geq 0$, the objective function of $P3$ (1) is a convex function of \mathbf{q} .

Proof. We prove Lemma 1 by induction. Let $E|_{K=n}$ be the energy consumption along the path (1) when $K = n$: $\sum_{k=1}^n c_1 \frac{\|q_k - q_{k-1}\|_2^2}{\Delta_t} + c_2 \|q_k - q_{k-1}\|_2 + c_3 \Delta_t$. We first prove that $E|_{K=1}$ is convex and then, by assuming that convexity holds for $E|_{K=n-1}$ we prove that $E|_{K=n}$ is a convex function of $\mathbf{q} = [q_0, \dots, q_n]$. It is easy to show that $E|_{K=1} = c_1 \frac{\|q_1 - q_0\|_2^2}{\Delta_t} + c_2 \|q_1 - q_0\|_2 + c_3 \Delta_t$ is a convex function of q_0 and q_1 because it consists of the sum of two convex functions, i.e., $c_1 \frac{\|q_1 - q_0\|_2^2}{\Delta_t}$ and $c_2 \|q_1 - q_0\|_2$, and a constant term. Assume that $E|_{K=n-1}$ is convex, then we have that $E|_{K=n} = E|_{K=n-1} + c_1 \frac{\|q_n - q_{n-1}\|_2^2}{\Delta_t} + c_2 \|q_n - q_{n-1}\|_2 + c_3 \Delta_t$. By following the same reasoning, we can observe that $E|_{K=n}$ is the sum of three convex functions of $\mathbf{q} = [q_0, \dots, q_n]$: $E|_{K=n-1}$ that is convex by hypothesis, $\frac{\|q_n - q_{n-1}\|_2^2}{\Delta_t}$, and $c_2 \|q_n - q_{n-1}\|_2$. \square

However, $P3$ is non-convex because the RHS of (15b) and (7e) are not concave functions of q_k . For this reason, we perform a convex local approximation of these two constraints and solve the problem iteratively by using an SCO algorithm. Starting from constraint (15b), we have the following:

Lemma 2: Given $\bar{A} \geq 0$, $\bar{B} \geq 0$, $\bar{C} \geq 0$, $\bar{\nu} \geq 0$, and $\bar{\mu} \geq 0$, $\bar{\mathbf{r}}^*$ is a convex function of $d_{a,k}$ and $d_{i,k}$ with $k = 0, \dots, K$.

Proof. See Appendix A. \square

Thus, since any convex function can be lower-bounded by its first-order Taylor expansion, we can write the following:

$$\begin{aligned} \bar{\mathbf{r}}^* &\geq \bar{\mathbf{r}}_{app}^* = \frac{1}{K} \sum_{k=0}^K \mathbf{r}_{app,k}^* = \\ &\frac{\mathbf{B}_w}{K} \sum_{k=0}^K \log_2 \left(1 + \left(\bar{A} d_{i,0,k}^{-\bar{\nu}} + \bar{B} d_{i,0,k}^{-\bar{\nu}/2} d_{a,0,k}^{-\bar{\mu}/2} + \bar{C} d_{a,0,k}^{-\bar{\mu}} \right) \frac{p_t}{\sigma^2} \right) + \\ &\nabla \bar{\mathbf{r}}^* \Big|_{(d_{a,0,k}, d_{i,0,k})}^T \begin{bmatrix} d_{a,k} - d_{a,0,k} \\ d_{i,k} - d_{i,0,k} \end{bmatrix}, \end{aligned} \quad (16)$$

where, $d_{a,0,k}$ and $d_{i,0,k}$ are the expansion points. The gradient (∇) with respect to $d_{a,k}$ and $d_{i,k}$ is given by:

$$\nabla \bar{\mathbf{r}}^* = \frac{\mathbf{B}_w}{K} \sum_{k=0}^K \begin{bmatrix} \frac{\left(-\bar{\nu} \bar{A} d_{i,k}^{-\bar{\nu}-1} - \bar{\nu}/2 \bar{B} d_{i,k}^{-\bar{\nu}/2-1} d_{a,k}^{-\bar{\mu}/2} \right) \frac{p_t}{\sigma^2}}{\ln 2 \left(1 + \left(\bar{A} d_{i,k}^{-\bar{\nu}} + \bar{B} d_{i,k}^{-\bar{\nu}/2} d_{a,k}^{-\bar{\mu}/2} + \bar{C} d_{a,k}^{-\bar{\mu}} \right) \frac{p_t}{\sigma^2} \right)} \\ \frac{\left(-\bar{\mu} \bar{C} d_{a,k}^{-\bar{\mu}-1} - \bar{\mu}/2 \bar{B} d_{i,k}^{-\bar{\nu}/2} d_{a,k}^{-\bar{\mu}/2-1} \right) \frac{p_t}{\sigma^2}}{\ln 2 \left(1 + \left(\bar{A} d_{i,k}^{-\bar{\nu}} + \bar{B} d_{i,k}^{-\bar{\nu}/2} d_{a,k}^{-\bar{\mu}/2} + \bar{C} d_{a,k}^{-\bar{\mu}} \right) \frac{p_t}{\sigma^2} \right)} \end{bmatrix}. \quad (17)$$

We now consider the following lemma:

Lemma 3: Given $d_{i,k} = \|q_k - q_i\|_2$ and $d_{a,k} = \|q_k - q_a\|_2$ and non-negative parameters \bar{A} , \bar{B} , \bar{C} , $\bar{\nu}$, and $\bar{\mu}$, $\bar{\mathbf{r}}_{app}^*$ is a concave function of q_k .

Proof. See Appendix B. \square

Thus, in a small neighborhood of $d_{a,0,k}$ and $d_{i,0,k}$, we can approximate $\bar{\mathbf{r}}^*$ with a concave function of q_k given by $\bar{\mathbf{r}}_{app}^*$. The same reasoning can be applied to (7e) leading to the following inequality:

$$\begin{aligned} (q_k - q_{c,o})^T P_o^{-1} (q_k - q_{c,o}) &\geq \\ (q_{0,k} - q_{c,o})^T P_o^{-1} (q_{0,k} - q_{c,o}) &+ \\ (q_{0,k} - q_{c,o})^T P_o^{-1} (q_k - q_{0,k}), \end{aligned} \quad (18)$$

where, the RHS is the first-order Taylor expansion of (7e) with respect to q_k at local point $q_{0,k}$. This is an affine function of q_k . Finally, by considering (16), (18) and a starting from a feasible initial trajectory \mathbf{q}_0 , we can solve a sequence of local convex approximations of $P3$, as shown in Algorithm 1. At each iteration j , Algorithm 1 solves the following problem:

$$P4 : \min_{\mathbf{q}_j} \sum_{k=1}^K c_1 \frac{\|q_{j,k} - q_{j,k-1}\|_2^2}{\Delta_t} + c_2 \|q_{j,k} - q_{j,k-1}\|_2 + c_3 \Delta_t \quad (19a)$$

$$\text{s.t.: } \bar{\mathbf{r}}_{app,j}^* \geq \mathbf{r}_{min}, \quad (19b)$$

$$\|q_{j,k} - q_{j,k-1}\|_2 \leq D_{max}, \quad \forall k, \quad (19c)$$

$$q_0 = q_s, \quad q_k = q_d, \quad (19d)$$

$$\|q_{j,k} - q_{j-1,k}\|_2 \leq T, \quad \forall k, \quad (19e)$$

$$\begin{aligned} (q_{j-1,k} - q_{c,o})^T P_o^{-1} (q_{j-1,k} - q_{c,o}) &+ \\ (q_{j-1,k} - q_{c,o})^T P_o^{-1} (q_{j,k} - q_{j-1,k}) &\geq d_s, \quad \forall k, o, \end{aligned} \quad (19f)$$

where, $\mathbf{q}_j = [q_{j,0}, q_{j,1}, \dots, q_{j,K}]$ and $\mathbf{q}_{j-1} = [q_{j-1,0}, q_{j-1,1}, \dots, q_{j-1,K}]$ are the solutions of $P4$ at iteration j and $j-1$, respectively. More precisely, \mathbf{q}_{j-1} represents the local point at which the approximations at iteration j of constraints (15b) and (7e) are computed. These approximations are valid in a trust region of \mathbf{q}_{j-1} (T) that is defined by constraint (19e). Note that the expansion points of $\bar{\mathbf{r}}^*$ can be obtained from $q_{j-1,k}$, as $d_{i,k} = \sqrt{(z_r - zi)^2 + \|q_{j-1,k} - q_i\|_2^2}$, and $d_{a,k} = \sqrt{(z_r - za)^2 + \|q_{j-1,k} - q_a\|_2^2}$. Problem $P4$ is convex and it can be solved quickly by interior-point methods. Algorithm 1 stops if the sequence of solutions converges or when a maximum number of iterations (N_{it}) is reached. Specifically, we can prove the following:

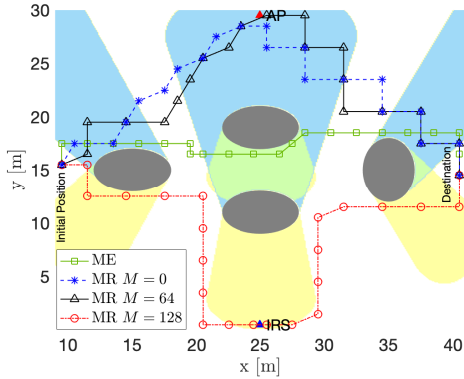


Fig. 2: Minimum energy (ME) and maximum rate (MR) initial solutions for $K = 30$ and several values of M . Yellow, blue, and green shaded positions are in NLOS with respect to the AP, the IRS, and both, respectively. The positions in the white area are in LOS with respect to both the IRS and the AP.

Theorem 1. *Algorithm 1 provides a sequence of solutions that is non-increasing and converges to a KKT point of $P3$.*

Proof. The convergence of Algorithm 1 to a KKT point of $P3$ follows from [10]. Moreover, the sequence of solutions provided by Algorithm 1 is non increasing because, the solution of $P4$ at iteration $j - 1$, \mathbf{q}_{j-1} , is a feasible solution of minimization problem $P4$ at iteration j . \square

Algorithm 1 QoS Constrained Robot Trajectory Planning

Initial solution:

- 1: $j=0$ and find an initial feasible solution \mathbf{q}_j
- 2: Compute the motion energy consumption E_j corresponding to \mathbf{q}_j as in (19a)

SCO:

- 3: **repeat**
- 4: $j = j + 1$
- 5: Obtain \mathbf{q}_j and E_j by solving $P4$ with local points \mathbf{q}_{j-1}
- 6: **until** $\frac{E_j - E_{j-1}}{E_{j-1}} \leq \epsilon$ or $j \geq N_{it}$

We consider two initial solutions for Algorithm 1 that are obtained by computing the shortest path on a time expanded graph as done in [11]. The edges and vertices of the graph are defined on a discrete set of positions that are free from obstacles. Then, by using the radio map, the costs of the edges are set to generate a first solution that minimizes the motion energy consumption (ME) and a second solution that maximizes the rate (MR). Algorithm 1 uses ME if this is feasible and MR, otherwise. If also the latter is not feasible, the algorithm declares infeasibility.

V. NUMERICAL RESULTS

In this section, we provide a numerical validation of Algorithm 1 for solving $P3$. For our simulations, we consider a $50 \times 30 \text{ m}^2$ rectangular-shaped indoor scenario. The robot's starting position is $[9.5, 15.5]$, whereas the destination is $[40.5, 14.5]$. Ellipse obstacles, with length, width, and height of 6 m, 4 m, and 2 m, respectively, are placed as in Fig. 2, where they are represented by gray shaded areas. In this scenario, there is an AP and an IRS placed at $[25, 30]$ and $[25, 0]$, respectively, operating in the 60 GHz band as in [12], with bandwidth $B_w = 200$ MHz. The height of the AP is 5 m, whereas, we set the heights of the IRS and the robot's

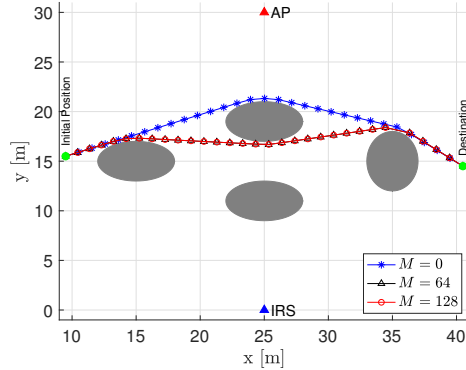


Fig. 3: Robot trajectories to which Algorithm 1 converges for $r_{min} = 2$ Gbps and several values of M .

antenna equal to 2.5 and 0.5 m, respectively. This scenario includes several robot-AP and robot-IRS channel conditions, i.e., LOS and NLOS positions. NLOS positions with respect to the AP, the IRS, and both are represented in Fig. 2 by yellow, blue, and green shaded areas, respectively.

In Fig. 2, we also show ME and MR initial solutions for several values of M . Note that MR initial solutions consider trajectories that avoid NLOS areas with respect to either the AP or to the IRS according to the number of reflective elements of the latter. Similar to [12], the path loss at a reference distance of 1 meter is 68 dB, and the path loss exponent of the robot-AP and robot-IRS channels are set to 2, for LOS cases, and 4.5, for positions in NLOS. The path loss exponent of the IRS-AP channel is set to 2. Moreover, we set the transmit and the noise powers to 20 dBm, and -80 dBm, respectively. We show the results, for several values of M and r_{min} , and we set the following parameters as follows: $N = 16$, $K = 30$, $\Delta_t = 1$ s, $v_{max} = 3$ m/s, $d_s = 1.35$, $N_{it} = 100$, $\epsilon = 0.01$, $T = 1$ m, $c_1 = 4.39$, $c_2 = 24.67$, and $c_3 = 14.77$ [6]. Finally, we can obtain (13) by estimating $\hat{A} \geq 0$, $\hat{B} \geq 0$, $\hat{C} \geq 0$, $\hat{v} \geq 0$, and $\hat{\mu} \geq 0$ by fitting (12) on a radio map by solving a non-linear least squares problem. The radio map is obtained from the average of 10.000 channel measurements on a grid of 500×300 points.

In Fig. 3, we show robot trajectories resulting from Algorithm 1 for $r_{min} = 2$ Gbps and several values of M . For $M = 0$, we can observe that the robot avoids NLOS areas with respect to the AP, and Algorithm 1 uses initial solution MR. When M increases, the IRS enhances the coverage and the robot can find a trajectory with lower energy consumption by using initial solution ME. The resulting trajectory crosses the NLOS area with respect to both the AP and the IRS. Note that, for $r_{min} = 2$ Gbps, values of M that are higher than 64 do not provide further gain, and the trajectories for $M = 64$ and $M = 128$ coincide.

This can be better observed in Fig. 4, where we show the energy consumption corresponding to the sequence of solutions \mathbf{q}_j provided by Algorithm 1 for several values of M and r_{min} . First, we can observe that the energy consumption corresponding to the sequence of solutions is non-increasing and Algorithm 1 converges in few iterations. Moreover, by increasing the number of reflective elements at the IRS M ,

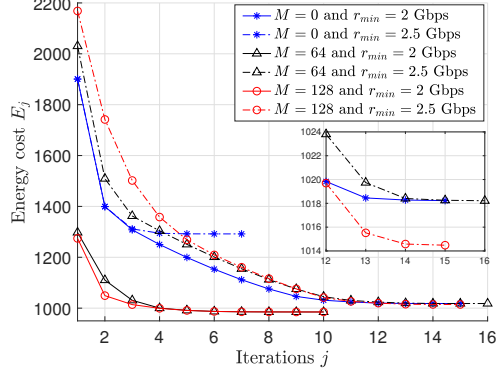


Fig. 4: Energy consumption corresponding to the sequence of solutions \mathbf{q}_j provided by Algorithm 1 for several values of M and r_{min} .

the robot can find paths with lower energy consumptions. The energy consumption increases for higher values of r_{min} . This can be better observed in Fig. 5, where we show robot trajectories resulting from Algorithm 1 for $r_{min} = 2.5$ Gbps, and several values of M . Specifically, when r_{min} increases, the robot must find paths that are closer to the AP and the IRS to improve the coverage and increase the data rate. Specifically, for all the values of M , Algorithm 1 selects MR initial solutions. For $M = 0$ and $M = 64$ the robot trajectories avoid NLOS areas with respect to the AP, whereas, for $M = 128$, paths that are closer to the IRS provide higher rates.

VI. CONCLUSION

In this work, we have proposed a novel robot trajectory optimization problem with QoS constrained communications for minimizing the motion energy consumption. The robot must avoid collisions with obstacles, reach the destination within a deadline, and transmit uplink data to an AP operating at mm-wave frequency bands and assisted by an IRS. We have proposed a solution that accounts for the mutual dependence between the channel conditions and the robot trajectory. Specifically, by exploiting the mm-wave propagation characteristics, we have decoupled the beamforming (at the AP and IRS) and the trajectory optimization problems. The latter is solved by an SCO algorithm for which the convergence to a KKT point is proved. Moreover, given a radio map, the proposed solution can find trajectories that avoid obstacles collisions and adapt to the propagation characteristics of the scenario. Specifically, we have shown how the number of IRS's reflective elements affects the robot trajectory. Future works will investigate the impact of the tasks' deadline on the solution and will consider more scenarios.

APPENDIX A

To prove Lemma 2, we prove that r_k^* , which is the estimated rate at timeslot k , is a convex function of $d_{i,k}$ and $d_{a,k}$. Then, \bar{r}^* is convex because it is a sum of convex functions. We first

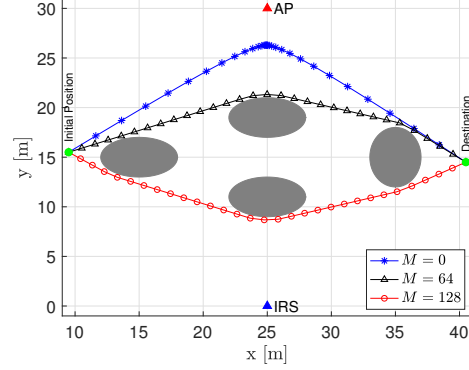


Fig. 5: Robot's trajectories to which Algorithm 1 converges for $r_{min} = 2.5$ Gbps and several values of M .

compute the partial derivatives of r_k^* with respect to $d_{i,k}$ and $d_{a,k}$. These are given by:

$$\frac{\partial r_k^*}{\partial d_{i,k}} = \frac{\left(-\bar{\nu} \bar{A} d_{i,k}^{-\bar{\nu}-1} - \bar{\nu}/2 \bar{B} d_{i,k}^{-\bar{\nu}/2-1} d_{a,k}^{-\bar{\mu}/2} \right) \frac{p_t}{\sigma^2}}{F_k}, \quad (20)$$

$$\frac{\partial r_k^*}{\partial d_{a,k}} = \frac{\left(-\bar{\mu} \bar{C} d_{a,k}^{-\bar{\mu}-1} - \bar{\mu}/2 \bar{B} d_{i,k}^{-\bar{\nu}/2} d_{a,k}^{-\bar{\mu}/2-1} \right) \frac{p_t}{\sigma^2}}{F_k}, \quad (21)$$

where, $F_k = \ln(2) \left(1 + \left(\bar{A} d_{i,k}^{-\bar{\nu}} + \bar{B} d_{i,k}^{-\bar{\nu}/2} d_{a,k}^{-\bar{\mu}/2} + \bar{C} d_{a,k}^{-\bar{\mu}} \right) \frac{p_t}{\sigma^2} \right) > 0$. Then, the second order partial derivatives are given by:

$$\frac{\partial^2 r_k^*}{\partial d_{i,k}^2} = \frac{\left(\bar{\nu}(\bar{\nu}+1) \bar{A} d_{i,k}^{-\bar{\nu}-2} + \bar{\nu}/2(\bar{\nu}/2+1) \bar{B} d_{i,k}^{-\bar{\nu}/2-2} d_{a,k}^{-\bar{\mu}/2} \right) F_k \frac{p_t}{\sigma^2}}{F_k^2} - \frac{\ln(2) \left(-\bar{\nu} \bar{A} d_{i,k}^{-\bar{\nu}-1} - \bar{\nu}/2 \bar{B} d_{i,k}^{-\bar{\nu}/2-1} d_{a,k}^{-\bar{\mu}/2} \right)^2 \frac{p_t^2}{\sigma^4}}{F_k^2}, \quad (22)$$

$$\frac{\partial^2 r_k^*}{\partial d_{a,k}^2} = \frac{\left(\bar{\mu}(\bar{\mu}+1) \bar{C} d_{a,k}^{-\bar{\mu}-2} + \bar{\mu}/2(\bar{\mu}/2+1) \bar{B} d_{i,k}^{-\bar{\nu}/2} d_{a,k}^{-\bar{\mu}/2-2} \right) F_k \frac{p_t}{\sigma^2}}{F_k^2} - \frac{\ln(2) \left(-\bar{\mu} \bar{C} d_{a,k}^{-\bar{\mu}-1} - \bar{\mu}/2 \bar{B} d_{i,k}^{-\bar{\nu}/2} d_{a,k}^{-\bar{\mu}/2-1} \right)^2 \frac{p_t^2}{\sigma^4}}{F_k^2}, \quad (23)$$

$$\frac{\partial^2 r_k^*}{\partial d_{i,k} \partial d_{a,k}} = \frac{\left((\bar{\mu}/2)(\bar{\nu}/2) \bar{B} d_{i,k}^{-\bar{\nu}/2-1} d_{a,k}^{-\bar{\mu}/2-1} \right) F_k \frac{p_t}{\sigma^2}}{F_k^2} - \frac{\ln(2) \left(-\bar{\nu} \bar{A} d_{i,k}^{-\bar{\nu}-1} - \bar{\nu}/2 \bar{B} d_{i,k}^{-\bar{\nu}/2-1} d_{a,k}^{-\bar{\mu}/2} \right) \frac{p_t^2}{\sigma^4}}{F_k^2} \times \frac{\left(-\bar{\mu} \bar{C} d_{a,k}^{-\bar{\mu}-1} - \bar{\mu}/2 \bar{B} d_{i,k}^{-\bar{\nu}/2} d_{a,k}^{-\bar{\mu}/2-1} \right) \frac{p_t^2}{\sigma^4}}{F_k^2}. \quad (24)$$

We can verify that $\frac{\partial^2 \mathbf{r}_k^*}{\partial d_{i,k}^2} > 0$, $\frac{\partial^2 \mathbf{r}_k^*}{\partial d_{a,k}^2} > 0$ and $\frac{\partial^2 \mathbf{r}_k^*}{\partial d_{i,k}^2} \frac{\partial^2 \mathbf{r}_k^*}{\partial d_{a,k}^2} - \left(\frac{\partial^2 \mathbf{r}_k^*}{\partial d_{i,k} \partial d_{a,k}} \right)^2 > 0$. Therefore, the Hessian is positive definite and \mathbf{r}_k^* is a convex function of $d_{i,k}$ and $d_{a,k}$.

APPENDIX B

We prove Lemma 3 by following the same reasoning of Appendix A. Note that $\bar{\mathbf{r}}_{app}^*$ in (16) is the sum of $K + 1$ functions each of them depending only on the robot's position at timeslot k :

$$\bar{\mathbf{r}}_{app}^* = \frac{1}{K} \sum_{k=0}^K \mathbf{r}_{app,k}^* = \quad (25)$$

$$\begin{aligned} & \frac{1}{K} \sum_{k=0}^K B_w \log_2 \left(1 + \left(\bar{A} d_{i,0,k}^{-\bar{\nu}} + \bar{B} d_{i,0,k}^{-\bar{\nu}/2} d_{a,0,k}^{-\bar{\mu}/2} + \bar{C} d_{a,0,k}^{-\bar{\mu}} \right) \frac{P_t}{\sigma^2} \right) \\ & - \frac{\partial \mathbf{r}_k^*}{\partial d_{a,k}} \Big|_{(d_{a,0,k}, d_{i,0,k})} d_{a,0,k} - \frac{\partial \mathbf{r}_k^*}{\partial d_{i,k}} \Big|_{(d_{a,0,k}, d_{i,0,k})} d_{i,0,k} \\ & + \frac{\partial \mathbf{r}_k^*}{\partial d_{a,k}} \Big|_{(d_{a,0,k}, d_{i,0,k})} \sqrt{(z_r - z_a)^2 + (x_k - x_a)^2 + (y_k - y_a)^2} \\ & + \frac{\partial \mathbf{r}_k^*}{\partial d_{i,k}} \Big|_{(d_{a,0,k}, d_{i,0,k})} \sqrt{(z_r - z_i)^2 + (x_k - x_i)^2 + (y_k - y_i)^2}, \end{aligned}$$

where, $\frac{\partial \mathbf{r}_k^*}{\partial d_{i,k}} < 0$ and $\frac{\partial \mathbf{r}_k^*}{\partial d_{a,k}} < 0$ are given by (20) and (21), respectively. Note that in (25) we have replaced q_k with $[x_k, y_k]$. Let us define $D_k = \sqrt{(z_r - z_a)^2 + (x_k - x_a)^2 + (y_k - y_a)^2}$, then, we can compute the partial derivatives of $\mathbf{r}_{app,k}^*$ with respect to x_k and y_k as follows:

$$\begin{aligned} \frac{\partial \mathbf{r}_{app,k}^*}{\partial x_k} &= \frac{\partial \mathbf{r}_k^*}{\partial d_{a,k}} \Big|_{(d_{a,0,k}, d_{i,0,k})} \frac{(x_k - x_a)}{D_k} + \\ & \frac{\partial \mathbf{r}_k^*}{\partial d_{i,k}} \Big|_{(d_{a,0,k}, d_{i,0,k})} \frac{(x_k - x_i)}{D_k}, \end{aligned} \quad (26)$$

$$\begin{aligned} \frac{\partial \mathbf{r}_{app,k}^*}{\partial y_k} &= \frac{\partial \mathbf{r}_k^*}{\partial d_{a,k}} \Big|_{(d_{a,0,k}, d_{i,0,k})} \frac{(y_k - y_a)}{D_k} + \\ & \frac{\partial \mathbf{r}_k^*}{\partial d_{i,k}} \Big|_{(d_{a,0,k}, d_{i,0,k})} \frac{(y_k - y_i)}{D_k}. \end{aligned} \quad (27)$$

The second order partial derivatives are given by:

$$\begin{aligned} \frac{\partial^2 \mathbf{r}_{app,k}^*}{\partial x_k^2} &= \frac{\partial \mathbf{r}_k^*}{\partial d_{a,k}} \Big|_{(d_{a,0,k}, d_{i,0,k})} \frac{(y_k - y_a)^2 + (z_k - z_a)^2}{D_k^3} + \\ & \frac{\partial \mathbf{r}_k^*}{\partial d_{i,k}} \Big|_{(d_{a,0,k}, d_{i,0,k})} \frac{(y_k - y_i)^2 + (z_k - z_i)^2}{D_k^3}, \end{aligned} \quad (28)$$

$$\begin{aligned} \frac{\partial^2 \mathbf{r}_{app,k}^*}{\partial y_k^2} &= \frac{\partial \mathbf{r}_k^*}{\partial d_{a,k}} \Big|_{(d_{a,0,k}, d_{i,0,k})} \frac{(x_k - x_a)^2 + (z_k - z_a)^2}{D_k^3} + \\ & \frac{\partial \mathbf{r}_k^*}{\partial d_{i,k}} \Big|_{(d_{a,0,k}, d_{i,0,k})} \frac{(x_k - x_i)^2 + (z_k - z_i)^2}{D_k^3}, \end{aligned} \quad (29)$$

$$\begin{aligned} \frac{\partial^2 \mathbf{r}_{app,k}^*}{\partial x_k \partial y_k} &= \frac{\partial \mathbf{r}_k^*}{\partial d_{a,k}} \Big|_{(d_{a,0,k}, d_{i,0,k})} \frac{(x_k - x_a)(y_k - y_a)}{D_k^3} + \\ & \frac{\partial \mathbf{r}_k^*}{\partial d_{i,k}} \Big|_{(d_{a,0,k}, d_{i,0,k})} \frac{(x_k - x_i)(y_k - y_i)}{D_k^3}. \end{aligned} \quad (30)$$

Note that $\frac{\partial^2 \mathbf{r}_{app,k}^*}{\partial x_k^2} < 0$ and $\frac{\partial^2 \mathbf{r}_{app,k}^*}{\partial y_k^2} < 0$ because $\frac{\partial \mathbf{r}_k^*}{\partial d_{i,k}} \Big|_{(d_{a,0,k}, d_{i,0,k})} < 0$ and $\frac{\partial \mathbf{r}_k^*}{\partial d_{a,k}} \Big|_{(d_{a,0,k}, d_{i,0,k})} < 0$ are negative terms $\forall d_{a,0,k} > 0, \forall d_{i,0,k} > 0$. Furthermore, we have that $\frac{\partial^2 \mathbf{r}_{app,k}^*}{\partial x_k^2} \frac{\partial^2 \mathbf{r}_{app,k}^*}{\partial y_k^2} - \left(\frac{\partial^2 \mathbf{r}_{app,k}^*}{\partial x_k \partial y_k} \right)^2 > 0$. Therefore, the Hessian is negative definite and $\mathbf{r}_{app,k}^*$ is a concave function of $q_k = [x_k, y_k]$.

REFERENCES

- [1] R. Sabella, A. Thuelig, M. C. Carrozza, and M. Ippolito, "Industrial automation enabled by robotics, machine intelligence and 5G," Ericsson Technology Review, 2018.
- [2] M. Giordani, M. Polese, M. Mezzavilla, S. Rangan, and M. Zorzi, "Toward 6G networks: Use cases and technologies," *IEEE Communications Magazine*, vol. 58, no. 3, pp. 55–61, 2020.
- [3] M. Cheffena, "Industrial wireless communications over the millimeter wave spectrum: opportunities and challenges," *IEEE Communications Magazine*, vol. 54, no. 9, pp. 66–72, Sep. 2016.
- [4] P. Wang, J. Fang, X. Yuan, Z. Chen, and H. Li, "Intelligent reflecting surface-assisted millimeter wave communications: Joint active and passive precoding design," *IEEE Transactions on Vehicular Technology*, pp. 1–1, 2020.
- [5] Yongguo Mei, Yung-Hsiang Lu, Y. C. Hu, and C. S. G. Lee, "Energy-efficient motion planning for mobile robots," in *IEEE International Conference on Robotics and Automation, Proceedings ICRA '04*, vol. 5, 2004, pp. 4344–4349 Vol.5.
- [6] Y. Yan and Y. Mostofi, "Co-optimization of communication and motion planning of a robotic operation under resource constraints and in fading environments," *IEEE Transactions on Wireless Communications*, vol. 12, no. 4, pp. 1562–1572, 2013.
- [7] Z. Xiao, P. Xia, and X. Xia, "Enabling UAV cellular with millimeter-wave communication: potentials and approaches," *IEEE Communications Magazine*, vol. 54, no. 5, pp. 66–73, 2016.
- [8] S. Li, B. Duo, X. Yuan, Y.-C. Liang, and M. D. Renzo, "Reconfigurable intelligent surface assisted UAV communication: Joint trajectory design and passive beamforming," 2019. [Online]. Available: <https://arxiv.org/abs/1908.04082>
- [9] X. Zhang, A. Liniger, and F. Borrelli, "Optimization-based collision avoidance," *IEEE Transactions on Control Systems Technology*, pp. 1–12, 2020.
- [10] B. R. Marks and G. P. Wright, "A general inner approximation algorithm for nonconvex mathematical programs," *Operations Research*, vol. 26, no. 4, pp. 681–683, 1978. [Online]. Available: <http://www.jstor.org/stable/169728>
- [11] C. Tatino, N. Pappas, and D. Yuan, "Multi-robot association-path planning in millimeter-wave industrial scenarios," 2020. [Online]. Available: <https://arxiv.org/abs/2003.09662>
- [12] S. Saponara, F. Giannetti, B. Neri, and G. Anastasi, "Exploiting mm-wave communications to boost the performance of industrial wireless networks," *IEEE Transactions on Industrial Informatics*, vol. 13, no. 3, pp. 1460–1470, 2017.